Figure S1

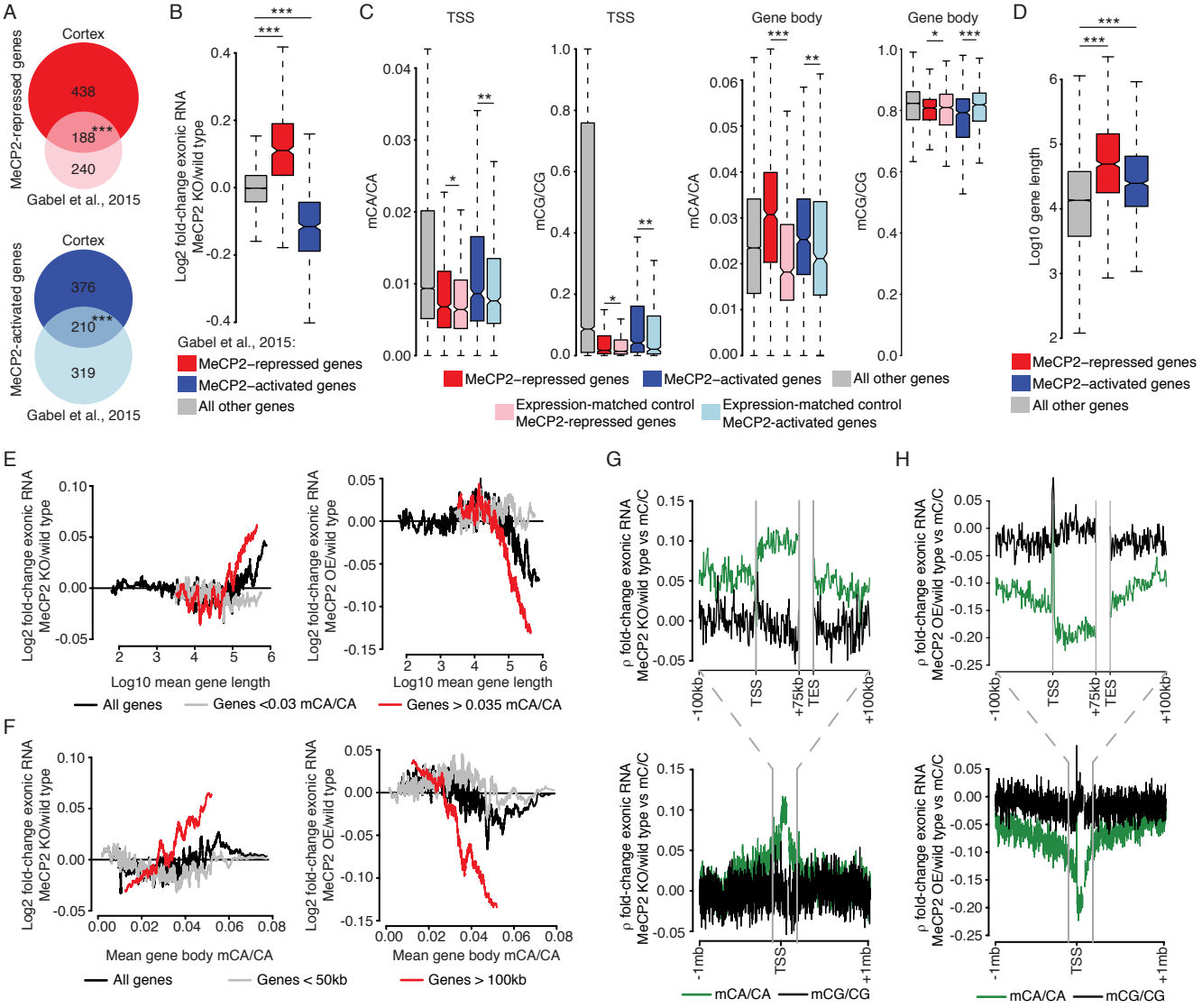

Figure S1. Identification of MeCP2-regulated genes in the cerebral cortex by combined RNA-seq analysis of MeCP2 KO and MeCP2 OE. Related to Figure 1.

A. Venn diagram of the overlap between genes identified as MeCP2-repressed and MeCP2-activated in combined analysis of MeCP2 KO and OE versus wild type cerebral cortex and genes previously identified as consistently dysregulated across multiple datasets and brain regions (Gabel et al., 2015). ***, $p < 10^{-8}$ hypergeometric test. Analysis was performed using coding genes found in annotation sets of both studies.

B. Boxplot of fold-changes in exonic RNA in the cortex of MeCP2 KO and wild type mice, for genes previously identified as consistently dysregulated across multiple datasets and brain regions (Gabel et al., 2015). ***, $p < 10^{-8}$ Wilcoxon rank-sum test.

C. Boxplots of mCA/CA and mCG/CG levels at the TSS (left) and gene bodies (right) of MeCP2-repressed, MeCP2-activated, and all other genes. Light colored boxplots are plots generated for a control set of genes matched for the distribution of gene expression for each dysregulated gene set (see methods). * $p < 0.05$; **, $p < 10^{-3}$; ***, $p < 10^{-8}$ Medians of Wilcoxon rank-sum tests on 100 gene-set resamplings.

D. Boxplot of gene lengths for MeCP2-repressed, MeCP2-activated, and all other genes identified in combined analysis of total RNA-seq from MeCP2 KO and OE cerebral cortex. ***, $p < 10^{-8}$ Wilcoxon rank-sum test.

E. Running average plots of exonic RNA fold-changes versus gene length, for MeCP2 KO (left) and OE (right) versus wild type. Mean fold-changes are plotted for bins of 201 genes sorted by gene length with a 1-gene step (see methods).

F. Running average plots of exonic RNA fold-change vs gene body mCA/CA for the MeCP2 KO (left) and OE (right) versus wild type. mCA/CA levels are calculated for the gene body defined as +3kb from the TSS to the TES. Mean fold-changes are plotted for bins of 201 genes sorted by mean mCA/CA per gene with a 1-gene step (see methods).

G. Plot of genome-wide correlations between methylation levels for 1kb regions in and around genes and fold-changes in exonic RNA expression in the MeCP2 KO versus wild type for each gene.

H. Plot of genome-wide correlations between methylation levels for 1kb regions in and around genes and fold-changes in exonic RNA expression in the MeCP2 OE versus wild type for each gene.

Data from cerebral cortex of 7-10 week old animals. n=6 per genotype for RNA-seq (MeCP2 KO, wild type), n=5 per genotype for RNA-seq (MeCP2 OE, wild type), n=2 wild type for DNA methylation (Stroud et al., 2017). In G and H analysis was carried out for genes over 75kb to visualize correlation signal within gene bodies.

Figure S2

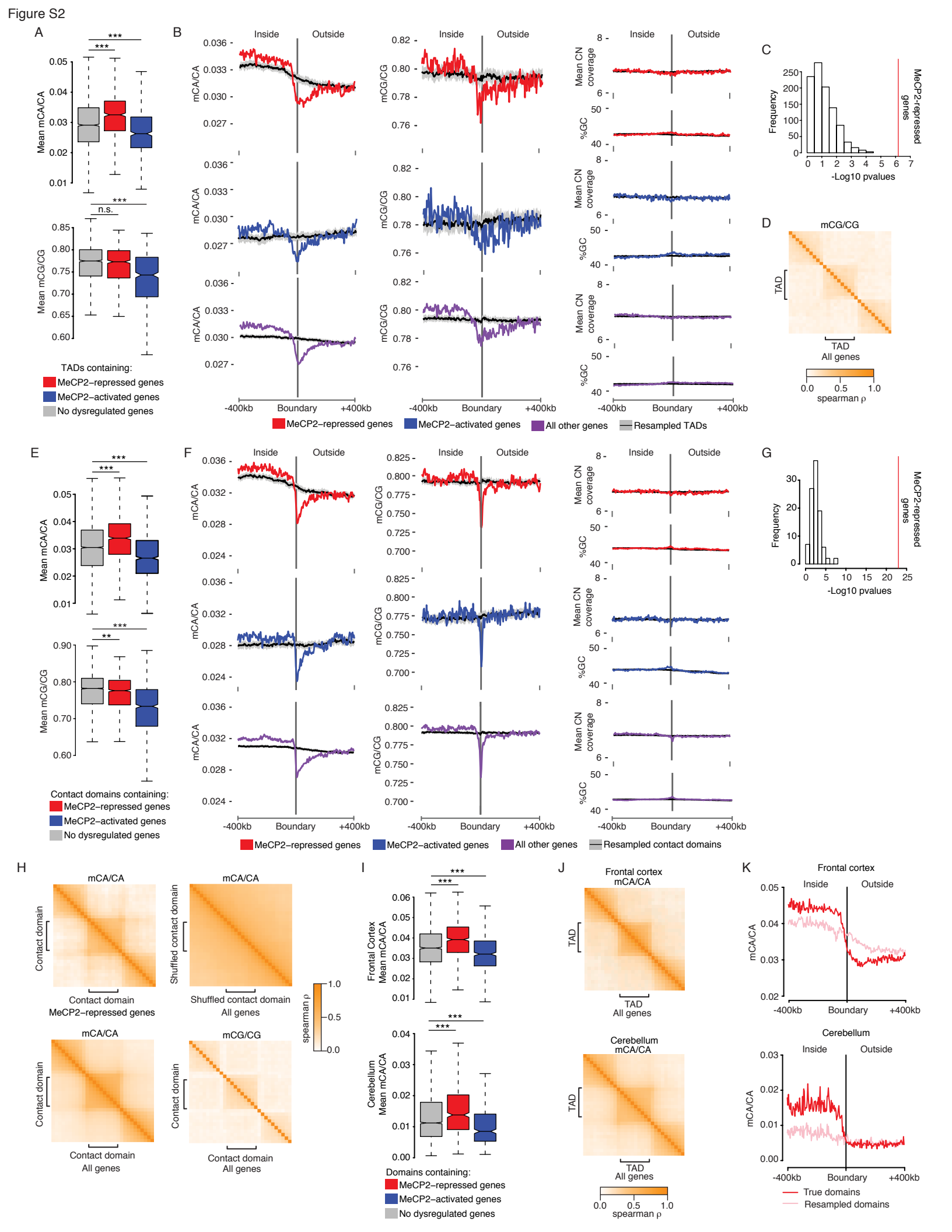
A
B
C
D
E
F
G
H
I
J
K
Mean mCA/CA
Mean mCG/CG
TADs containing:
MeCP2−repressed genes
MeCP2−activated genes
No dysregulated genes
Inside
Outside
mCA/CA
mCG/CG
Mean CN coverage
%GC
-400kb
Boundary
+400kb
MeCP2−repressed genes
MeCP2−activated genes
All other genes
Resampled TADs
Frequency
-Log10 pvalues
MeCP2-repressed genes
mCG/CG
TAD
All genes
spearman ρ
Contact domains containing:
Resampled contact domains
mCA/CA
mCG/CG
Contact domain
Shuffled contact domain
MeCP2−repressed genes
All genes
Frontal Cortex Mean mCA/CA
Cerebellum Mean mCA/CA
Domains containing:
Frontal cortex
Cerebellum
True domains
Resampled domains

Figure S2. Chromatin topology is associated with non-CG DNA methylation in the cerebral cortex. Related to Figure 1.

A. Boxplots of mCA/CA and mCG/CG within TADs that contain MeCP2-repressed genes, MeCP2-activated genes, or no dysregulated genes. ***, $p < 10^{-8}$ Wilcoxon rank-sum test.

B. Aggregate plots of mCA/CA (left), mCG/CG (center), and BS-sequencing coverage rates and GC composition (right) phased on boundaries of TADs defined in Hi-C data from the cerebral cortex at eight weeks of age. TADs containing MeCP2-repressed (red), MeCP2-activated (blue), or all other genes (purple) are shown. “Inside” indicates TADs containing genes of interest. Black line and ribbon for each plot indicates the mean and standard deviation of 20 sets of resampled boundaries generated by shuffling TAD locations in the genome (see methods).

C. A histogram of -log10 p-values for paired t-tests, comparing the difference in DNA methylation on either side of the TAD boundaries or 1000 resampled TAD boundaries as in B. Histogram shows the distribution of p-values for resampled TADs, red line indicates p-value for true TADs.

D. Cross correlation analysis of mCG/CG signal within and across TAD boundaries for all genes. mCG/CG values were calculated for 10 intra-domain regions and 10 equally-sized regions up and downstream of each TAD. Correlation between these regions across all TADs is shown (see methods).

E. Boxplots of mCA/CA and mCG/CG within contact domains that contain MeCP2-repressed genes, MeCP2-activated genes, or no dysregulated genes. Contact domains were defined by analysis of Hi-C data generated from cerebral cortex neurons isolated from fetal brain (Bonev et al., 2017). **,$p < 10^{-3}$; ***, $p < 10^{-8}$ Wilcoxon rank-sum test.

F. Aggregate plots of mCA/CA (left), mCG/CG (center), and BS-sequencing coverage rates and GC composition (right) phased on boundaries of contact domains defined in Hi-C data from fetal cortical neurons. Presented as in panel B.

G. A histogram of -log10 p-values for paired t-tests, comparing the difference in DNA methylation on either side of contact domain boundaries or 100 resampled contact domain boundaries as in panel F. Histogram shows the distribution of p-values for resampled contact domains, red line indicates p-value for true contact domains.

H. Cross correlation analysis of mCA/CA and mCG/CG signal within and outside of contact domains as in panel D. Resampling was performed by shuffling contact domain-sized regions around the genome and repeating the analysis of all genes (see methods).

I. Boxplots of mCA/CA within TADs defined in cerebral cortex (top) and cerebellum (bottom) that contain MeCP2-repressed genes, MeCP2-activated genes, or no dysregulated genes. ***, $p < 10^{-8}$ Wilcoxon rank-sum test. Cerebral cortex TADs were compared to genes from this study. Cerebellum TADs were compared to genes previously identified as misregulated in the cerebellum and multiple other brain regions (Gabel et al., 2015).

J. Cross correlation analysis of mCA/CA signal within and outside of TADs defined in cerebral cortex (top) and cerebellum (bottom), as performed in panel H.

K. Aggregate plots of mCA/CA from frontal cortex (top) and granule neurons (bottom) phased on boundaries of MeCP2 repressed TADs defined in cerebral cortex (top) and cerebellum (bottom). Analysis performed on TADs with highly differing mCA levels as in Figure 1G.

A-D analysis of Hi-C interaction data (Dixon et al., 2012), and DNA methylation, n=2 (Stroud et al., 2017) from the cerebral cortex at 8 weeks of age. E-H analysis of Hi-C interaction data from neurons isolated from E14.5 cortex (Bonev et al., 2017), and DNA methylation, n=2 (Stroud et al., 2017) from the cerebral cortex at 8 weeks of age. I-K analysis of bisulfite data from 6-week frontal cortex and granule neurons isolated from 7-12 week old cerebellum (Lister et al., 2013; Mellén et al., 2017)(Mellén et al., 2017). Hi-C data from 6-8 week old Cerebellum (Yamada et al., 2019). Note that some panels from Figure 1 are repeated here to allow for comparisons.

Figure S3

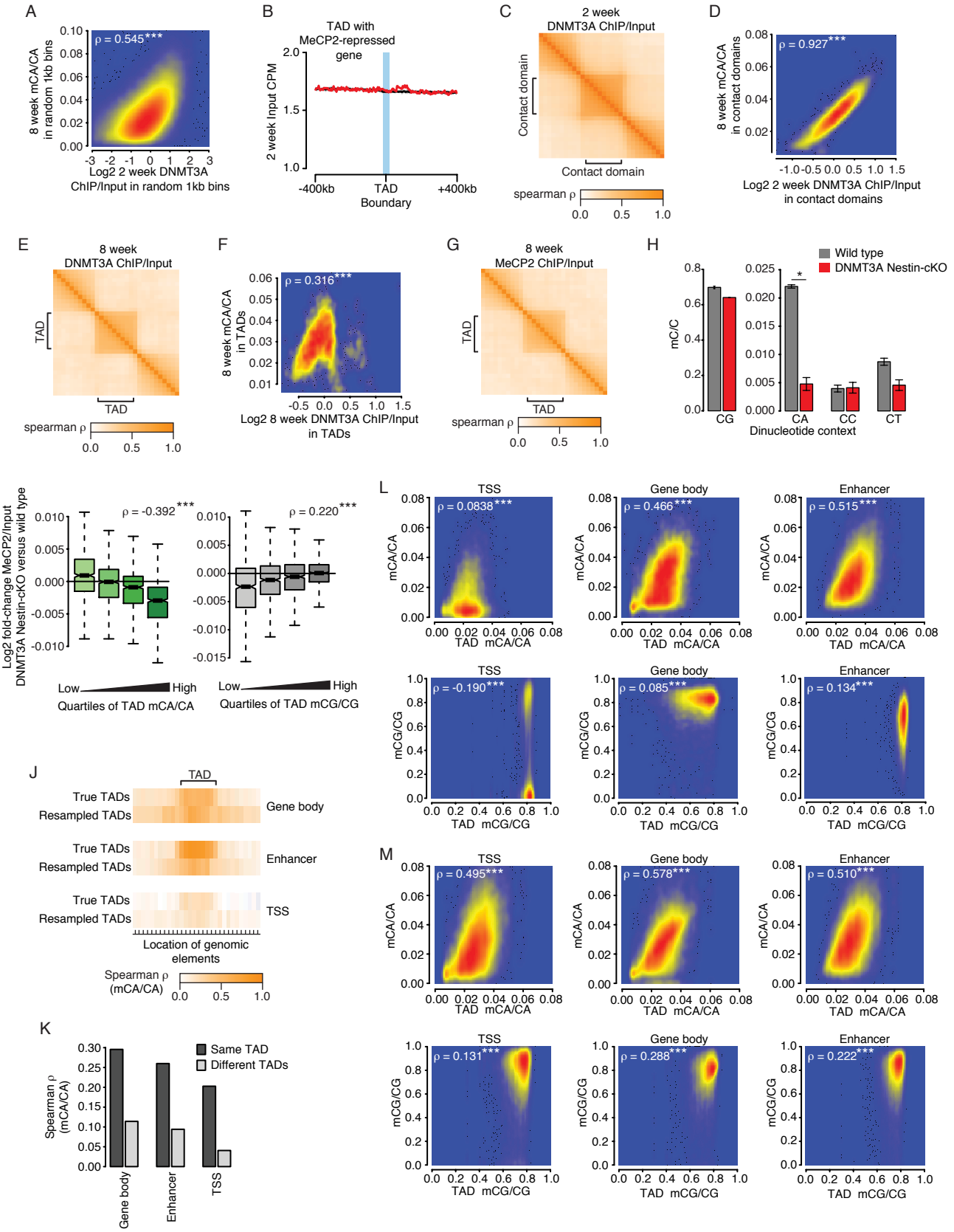
A
ρ = 0.545***
8 week mCA/CA in random 1kb bins
Log2 2 week DNMT3A ChIP/Input in random 1kb bins
B
TAD with MeCP2-repressed gene
2 week Input CPM
-400kb
TAD Boundary
+400kb
C
2 week DNMT3A ChIP/Input
Contact domain
spearman ρ
D
ρ = 0.927***
8 week mCA/CA in contact domains
Log2 2 week DNMT3A ChIP/Input in contact domains
E
8 week DNMT3A ChIP/Input
TAD
spearman ρ
F
ρ = 0.316***
8 week mCA/CA in TADs
Log2 8 week DNMT3A ChIP/Input in TADs
G
8 week MeCP2 ChIP/Input
H
Wild type
DNMT3A Nestin-cKO
mC/C
CG
CA
CC
CT
Dinucleotide context
I
Log2 fold-change MeCP2/Input DNMT3A Nestin-cKO versus wild type
ρ = -0.392***
ρ = 0.220***
Low
High
Quartiles of TAD mCA/CA
Quartiles of TAD mCG/CG
J
True TADs
Resampled TADs
Gene body
Enhancer
TSS
Location of genomic elements
Spearman ρ (mCA/CA)
K
Same TAD
Different TADs
Spearman ρ (mCA/CA)
L
TSS
Gene body
Enhancer
ρ = 0.0838***
ρ = 0.466***
ρ = 0.515***
ρ = -0.190***
ρ = 0.085***
ρ = 0.134***
TAD mCA/CA
TAD mCG/CG
M
ρ = 0.495***
ρ = 0.578***
ρ = 0.510***
ρ = 0.131***
ρ = 0.288***
ρ = 0.222***

Figure S3. Binding of DNMT3A and recruitment of MeCP2 are shaped by topologically-associating domains. Related to Figure 2.

A. Density scatter plot of DNMT3A ChIP/Input signal at 2 weeks of age and mCA/CA levels at 8 weeks of age for random 1kb regions of the genome. Spearman rho shown for the correlation between DNMT3A signal and mCA/CA level. ***, $p < 10^{-8}$.

B. Aggregate plot of Input CPM at 2 weeks phased on boundaries of TADs that contain MeCP2-repressed genes (TADS from cerebral cortex at eight weeks of age). Black line and ribbon for each plot indicates the mean and standard deviation of 20 resampled boundaries generated by shuffling contact domain locations in the genome (see methods).

C. Cross correlation analysis of DNMT3A ChIP-seq signal at 2 weeks of age for contact domains defined in fetal cortical neurons. DNMT3A ChIP/Input values were calculated for 10 intra-domain regions and 10 equally-sized regions up and downstream of each domain. Correlation between these regions across all domains is shown (see methods).

D. Density scatter plot of DNMT3A ChIP/Input signal at 2 weeks of age and mCA/CA levels at 8 weeks of age for contact domains defined in fetal cortical neurons. Spearman rho shown for the correlation between DNMT3A signal and mCA/CA level. ***, $p < 10^{-8}$.

E. Cross correlation analysis (performed as in panel C) for DNMT3A ChIP-seq signal at 8 weeks of age in TADs defined in the cortex at 8 weeks of age.

F. Density scatter plot of DNMT3A ChIP/Input signal at 8 weeks of age and mCA/CA levels at 8 weeks of age for TADs defined in the cortex at 8 weeks of age. Spearman rho shown for the correlation between DNMT3A signal and mCA/CA level. ***, $p < 10^{-8}$.

G. Cross correlation analysis (performed as in panel C) for MeCP2 ChIP/Input signal at 8 weeks of age in TADs defined in the cortex at 8 weeks of age.

H. Barplots of genome-wide mC/C levels in a DNMT3A Nestin-cKO and control cerebral cortex at 8 weeks of age. Data shown as means +\- SEM. *, $p < 0.05$ two-tailed t-test.

I. Boxplot of fold-changes in MeCP2 ChIP-seq signal within TADs upon ablation of mCA in the DNMT3A Nestin-cKO. Change in signal is shown for TADs separated by quartiles of mCA/CA (left) and mCG/CG (right) under wild-type conditions. Spearman rho shown for the correlation between DNMT3A signal and mCA/CA level. *** $p < 10^{-8}$.

J. Heatmap of correlation between mCA/CA levels of gene body (top), enhancer (middle), and TSS (bottom) regions found inside and outside of TADs and the average mCA/CA level for each TAD. Distinct drop off in correlation coefficient for these elements when they are found outside the TAD boundary illustrates influence of intra-TAD mCA/CA consistency. Similar correlation level and drop-off in signal is not seen for resampled TADs, placed in randomized positions in the genome (see methods).

K. Barplots of correlations of mCA/CA levels for gene bodies (left), enhancers (middle), and TSSs (right), located in either the same TAD or separate TADs. To facilitate comparison, distances between pairs of elements in different TADs was matched to distances between pairs of elements in the same TAD (see methods).

L. Density scatter plots of TAD methylation levels and methylation at kilobase-scale genomic elements in the cerebral cortex at 8 weeks of age. Values for every TSS, gene body, or enhancer in the genome are plotted against the TAD in which the element resides. As in Figure 2E, data is subtracted from TADs such that element methylation does not contribute to plotted TAD methylation. Spearman rho shown for the methylation levels of each genomic element versus the methylation levels of the TAD that the element is in. ***, $p < 10^{-8}$.

M. Density scatter plots of TAD methylation levels and methylation at resampled random locations for regions size-matched to kilobase-scale genomic elements (as in panel L). Values for every resampled TSS-, gene body-, or enhancer-sized region in the genome are plotted against the TAD in which the element resides. Spearman rho shown for the methylation levels of each randomized genomic element versus the methylation levels of the TAD that the element is in. ***, $p < 10^{-8}$.

A,C,D Analysis of Hi-C interaction data from neurons isolated from E14.5 cortex (Bonev et al., 2017), DNA methylation, n=2, from the cerebral cortex at 8 weeks of age, and DNMT3A ChIP-seq data, n=3, from the cerebral cortex at 2 weeks of age (Stroud et al., 2017). B,E-G,I-M Analysis of Hi-C interaction data (Dixon et al., 2012), DNA methylation (n=2 wild type), DNMT3A ChIP-seq data, (n=2 wild type), (Stroud et al., 2017), and MeCP2 ChIP-seq data (n=2 per genotype) (Kinde et al., 2016) from the cerebral cortex at 8 weeks of age. H n=2 per genotype for DNA methylation DNMT3A Nestin-cKO versus wild-type, 8 weeks of age. Note that some panels from Figure 2 are repeated to allow for comparisons.

Figure S4

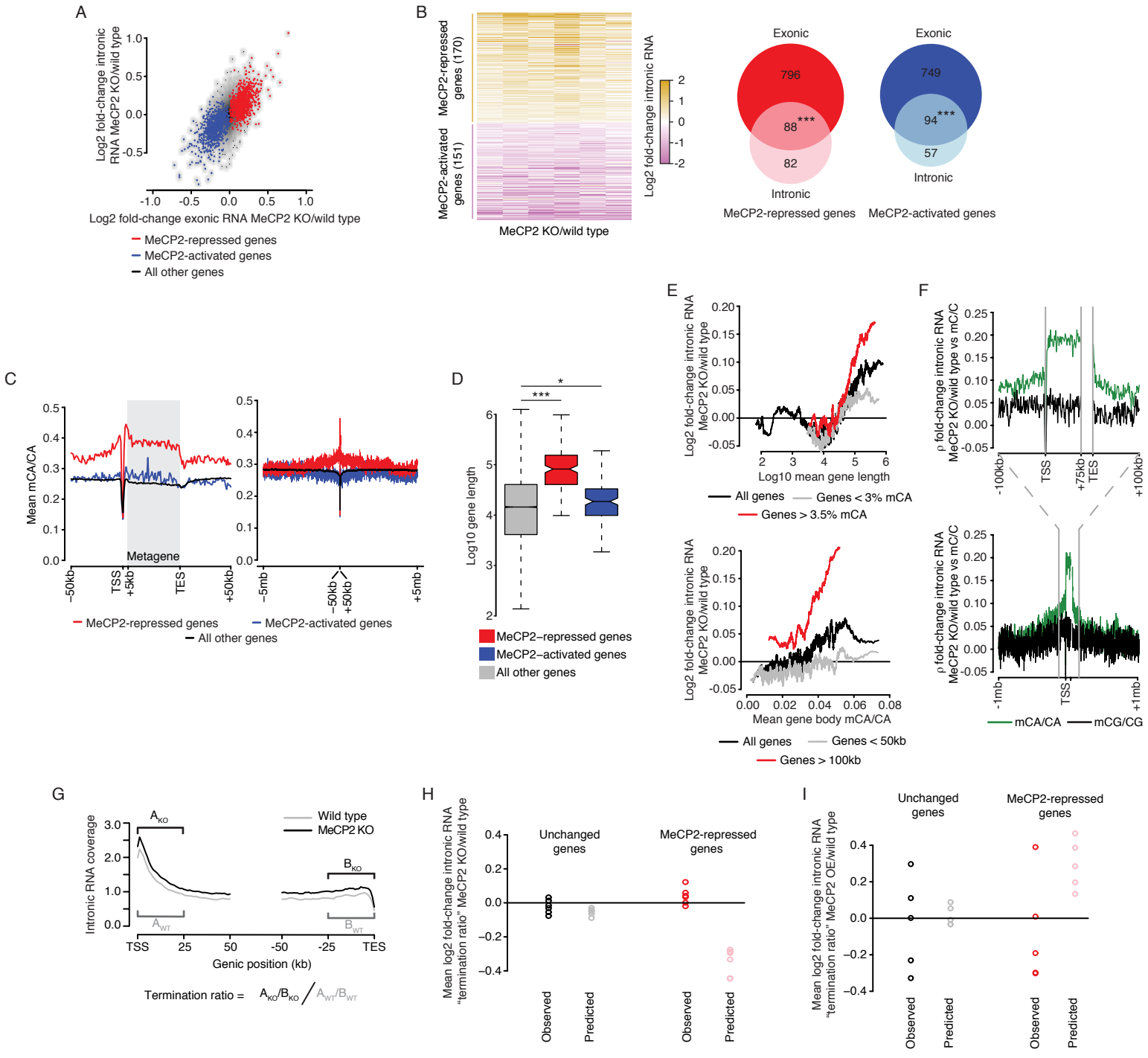
A
Log2 fold-change intronic RNA MeCP2 KO/wild type
Log2 fold-change exonic RNA MeCP2 KO/wild type
MeCP2-repressed genes
MeCP2-activated genes
All other genes
B
MeCP2-repressed genes (170)
MeCP2-activated genes (151)
Log2 fold-change intronic RNA
MeCP2 KO/wild type
Exonic
796
88***
82
Intronic
MeCP2-repressed genes
Exonic
749
94***
57
Intronic
MeCP2-activated genes
C
Mean mCA/CA
Metagene
MeCP2-repressed genes
MeCP2-activated genes
All other genes
D
Log10 gene length
MeCP2–repressed genes
MeCP2–activated genes
All other genes
E
Log2 fold-change intronic RNA MeCP2 KO/wild type
Log10 mean gene length
All genes
Genes < 3% mCA
Genes > 3.5% mCA
Mean gene body mCA/CA
Genes < 50kb
Genes > 100kb
F
ρ fold-change intronic RNA MeCP2 KO/wild type vs mC/C
mCA/CA
mCG/CG
G
Intronic RNA coverage
Wild type
MeCP2 KO
Genic position (kb)
Termination ratio =
H
Mean log2 fold-change intronic RNA "termination ratio" MeCP2 KO/wild type
Unchanged genes
MeCP2-repressed genes
Observed
Predicted
I
Mean log2 fold-change intronic RNA "termination ratio" MeCP2 OE/wild type
Unchanged genes
MeCP2-repressed genes
Observed
Predicted

Figure S4. Changes in intronic RNA are consistent with promoter-associated transcriptional upregulation of long, highly methylated, MeCP2-repressed genes in the MeCP2 KO. Related to Figure 3.

A. Scatterplot of the log2 fold-changes in the MeCP2 KO versus wild type for exonic RNA measured by total RNA sequencing of cerebral cortex tissue compared to intronic RNA measured by total RNA sequencing of isolated nuclei from this tissue. Genes identified as MeCP2-repressed and MeCP2-activated in combined analysis of exonic RNA in MeCP2 KO and MeCP2 OE mice (Figure 1; S1) are indicated by red and blue dots respectively, all other genes indicated as gray points.

B. Left, heatmap of changes in intronic RNA for genes detected as significantly dysregulated (FDR <0.1) in nuclear RNA-seq from MeCP2 KO cerebral cortex (grey indicates, no data for replicate). Right, venn diagram of the overlap between genes called as MeCP2-repressed or MeCP2-activated in analysis of nuclear intronic RNA expression in the MeCP2 KO (pale colors) with genes called as dysregulated in combined analysis of exonic RNA in the MeCP2 KO and MeCP2 OE mice (dark colors) (Figure 1; S1). ***, $p < 10^{-8}$ hypergeometric test.

C. Aggregate plot of cerebral cortex mCA/CA levels for MeCP2-repressed, MeCP2-activated, and all other genes defined by analysis of intronic RNA in the MeCP2 KO (see panel B). Mean mCA/CA for 1kb bins in the TSS and regions surrounding genes is shown. For “Metagene” region, mean mCA/CA was calculated for 50 equal-sized bins within the body of each gene.

D. Boxplot of gene lengths for MeCP2-repressed or MeCP2-activated, and all other genes called by analysis of nuclear intronic RNA in the MeCP2 KO and wild type mice. *, $p < 0.05$; ***, $p < 10^{-8}$ Wilcoxon rank-sum test.

E. Running-average plot of fold-changes in intronic RNA expression in the MeCP2 KO and wild type versus mean gene length (top) or mean gene body mCA/CA (bottom). Mean fold-changes are plotted for bins of 201 genes sorted by length of mCA/CA per gene with a 1-gene step (see methods).

F. Plot of spearman correlations between fold-changes in intronic RNA expression in the MeCP2 KO and wild type versus mCA/CA or mCG/CG for regions in and around genes. Analysis performed for 1kb bins across 200kb (top) and 2 Mb (bottom) regions.

G. Scheme to assess changes in pre-mature transcription termination in the MeCP2 KO versus wild type. Similar to analysis carried out by Boswell et al., 2017, a “termination ratio” for each gene above 50kb in each sample is defined as the ratio of read counts in the first 25kb of each gene to the read counts in the last 25 kb of that gene. The mean fold-change in the ratios between MeCP2 KO and wild type is calculated across all genes in paired replicates.

H. Dotplot showing the change in termination ratio between the nuclear intronic RNA-seq data in the MeCP2 KO and wild type for genes that are not significantly changed and MeCP2-repressed genes. A prediction for the change in this ratio that would be expected if the effects on mRNA in the MeCP2 KO were due entirely to changes in transcription termination rate was generated for comparison, “Predicted” (see methods).

I. Dotplot as in panel H, showing the change in termination ratio between the intronic RNA-seq in the MeCP2 OE and wild type for genes that are not significantly changed and MeCP2-repressed genes.

Data from cerebral cortex of 7-10 week old animals. For MeCP2 KO: n= 6 per genotype for RNA-seq; for MeCP2 OE: n=5 per genotype for RNA-seq; n=2 wild-type for DNA methylation (Stroud et al., 2017).

Figure S5

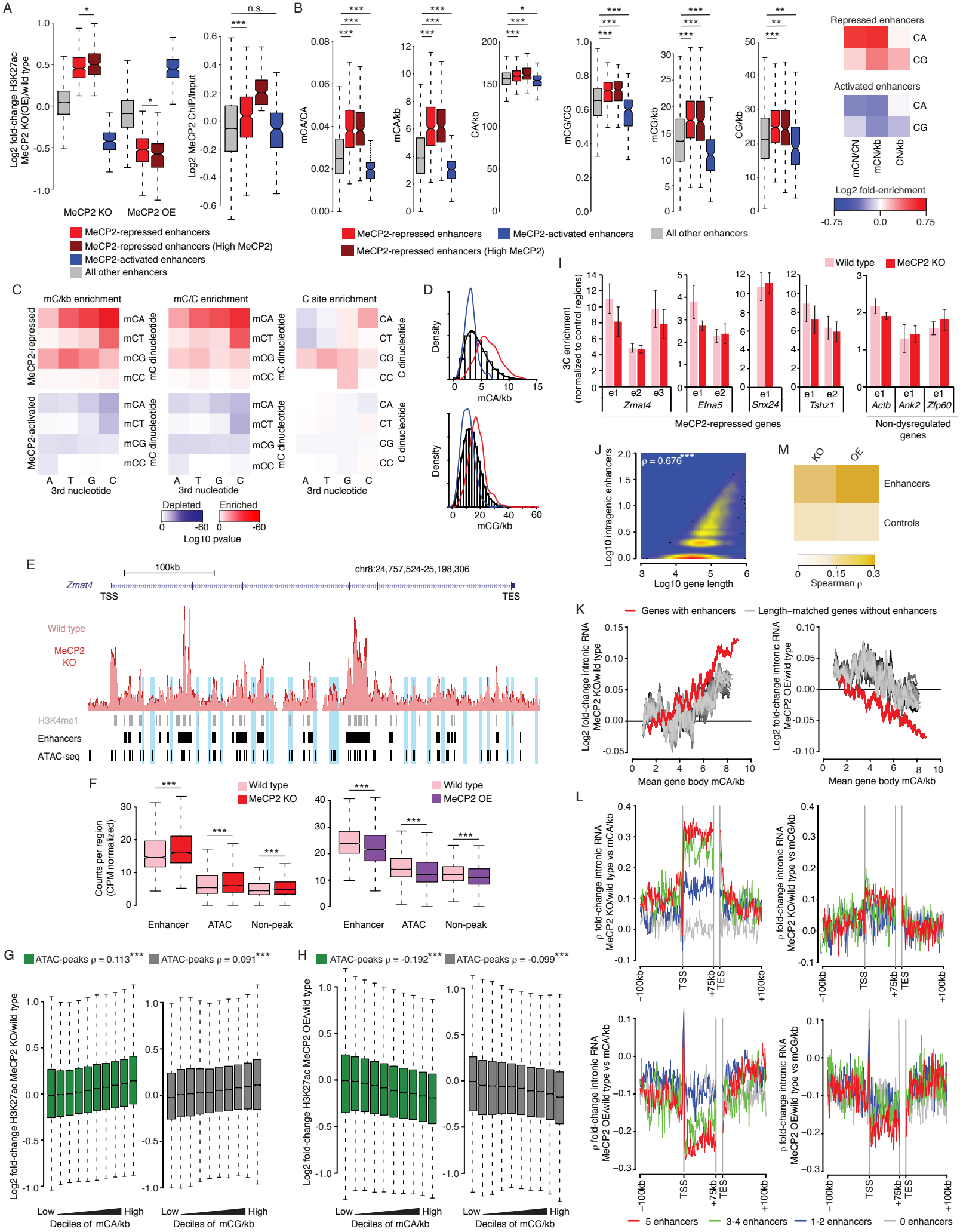
A
Log2 fold-change H3K27ac MeCP2 KO(OE)/wild type
MeCP2 KO
MeCP2 OE
Log2 MeCP2 ChIP/Input
n.s.
MeCP2-repressed enhancers
MeCP2-repressed enhancers (High MeCP2)
MeCP2-activated enhancers
All other enhancers
B
mCA/CA
mCA/kb
CA/kb
mCG/CG
mCG/kb
CG/kb
Repressed enhancers
Activated enhancers
CA
CG
mCN/CN
mCN/kb
CN/kb
Log2 fold-enrichment
C
mC/kb enrichment
mC/C enrichment
C site enrichment
MeCP2-repressed
MeCP2-activated
mC dinucleotide
C dinucleotide
3rd nucleotide
Depleted
Enriched
Log10 pvalue
D
Density
mCA/kb
mCG/kb
E
100kb
chr8:24,757,524-25,198,306
Zmat4
TSS
TES
Wild type
MeCP2 KO
H3K4me1
Enhancers
ATAC-seq
F
Wild type
MeCP2 KO
MeCP2 OE
Counts per region (CPM normalized)
Enhancer
ATAC
Non-peak
G
ATAC-peaks ρ = 0.113***
ATAC-peaks ρ = 0.091***
Log2 fold-change H3K27ac MeCP2 KO/wild type
Low
High
Deciles of mCA/kb
Deciles of mCG/kb
H
ATAC-peaks ρ = -0.192***
ATAC-peaks ρ = -0.099***
Log2 fold-change H3K27ac MeCP2 OE/wild type
I
Wild type
MeCP2 KO
3C enrichment (normalized to control regions)
Zmat4
Efna5
Snx24
Tshz1
Actb
Ank2
Zfp60
MeCP2-repressed genes
Non-dysregulated genes
J
ρ = 0.676***
Log10 intragenic enhancers
Log10 gene length
M
KO
OE
Enhancers
Controls
Spearman ρ
K
Genes with enhancers
Length−matched genes without enhancers
Log2 fold-change intronic RNA MeCP2 KO/wild type
Log2 fold-change intronic RNA MeCP2 OE/wild type
Mean gene body mCA/kb
L
ρ fold-change intronic RNA MeCP2 KO/wild type vs mCA/kb
ρ fold-change intronic RNA MeCP2 KO/wild type vs mCG/kb
ρ fold-change intronic RNA MeCP2 OE/wild type vs mCA/kb
ρ fold-change intronic RNA MeCP2 OE/wild type vs mCG/kb
−100kb
TSS
+75kb
TES
+100kb
5 enhancers
3-4 enhancers
1-2 enhancers
0 enhancers

Figure S5. Analysis of enhancers dysregulated in MeCP2 mutants. Related to Figure 4 and Figure 6.

A. Boxplot of fold-changes in H3K27ac ChIP signal in MeCP2 KO and OE (left) and MeCP2 ChIP/Input signal (right) for enhancers identified with combined ChIP-seq analysis in KO and OE as MeCP2-repressed, MeCP2-repressed with high MeCP2/Input (see methods), MeCP2-activated, or all other enhancers. Fold-changes were calculated by edgeR analysis of H3K27ac ChIP-seq signal at enhancer regions (see methods). Significantly dysregulated enhancers were defined as FDR < 0.1. *, $p < 0.05$, ***, $p < 10^{-8}$ Wilcoxon rank-sum test.

B. Left, boxplots of mC/C, mC/kb, and C sites/kb at MeCP2-repressed, MeCP2-repressed with high MeCP2, MeCP2-activated, and all other enhancers, as displayed in panel A. Right, heatmap of enrichments for median levels of mC/C, mC/kb, and C sites/kb for MeCP2-repressed and MeCP2-activated enhancers compared to all other enhancers. *, $p < 0.05$, **, $p < 10^{-3}$; ***, $p < 10^{-8}$ Wilcoxon rank-sum test.

C. Heatmap of enrichment significance for number of mC sites (mC/kb, left), methylation level (mC/C, middle) and sequence occurrence (right) for trinucleotide sites in MeCP2-repressed and MeCP2-activated enhancers. Significance of enrichment or depletion was calculated by comparing occurrences of mC/kb, mC/C, or sequence alone for each trinucleotide in the 2kb region surrounding enhancers to resampled sets of enhancers that are not significantly changed and matched to changed enhancers for H3K27ac signal (see methods).

D. Histograms of mCA/kb and mCG/kb in enhancers (black). Blue and red lines indicate the distributions of methylation for MeCP2-activated and MeCP2-repressed enhancers respectively.

E. Genome browser view of an example MeCP2-repressed gene, *Zmat4* (as in Figure 4A), showing overlaid wild-type and MeCP2 KO aggregate H3K27ac ChIP-seq signal, H3K4me1 ChIP-seq peaks, H3K27ac peaks called as enhancers, and peaks from a compendium of ATAC-seq peaks identified across 13 mouse tissues. Blue highlights ATAC-seq peaks that correspond to sub-thresholded enrichment of H3K27ac, not identified in peak calling analysis of H3K27ac ChIP-seq.

F. Boxplots of H3K27ac ChIP signal in MeCP2 KO versus wild type (left) and MeCP2 OE vs wild type (right) for enhancers defined in this study, a compendium of detectable ATAC-seq peaks, and non-peak regions that are sized matched to ATAC-peaks but selected to not overlap enhancers of ATAC-seq peaks. Values for the highest mCA/CA decile are shown for each class, illustrating total levels of H3K27ac and mCA-dependent dysregulation ***, $p < 10^{-8}$ Wilcoxon rank-sum test.

G. Boxplots of fold-changes of H3K27ac ChIP signal in MeCP2 KO versus wild type across deciles of mCA/kb (left) and mCG/kb (right) for ATAC-peaks described in panel E. Spearman rho shown for correlations of each methylation mark with change of H3K27ac at enhancers. ***, $p < 10^{-8}$ Wilcoxon rank-sum test.

H. Boxplots of fold-changes of H3K27ac ChIP signal in MeCP2 OE versus wild type across deciles of mCA/kb (left) and mCG/kb (right) for ATAC-peaks described in E. Spearman rho shown for correlations of each methylation mark with change of H3K27ac at enhancers. ***, $p < 10^{-8}$.

I. Quantitative 3C analysis of enhancers found in MeCP2 repressed genes, or control loci. Data shown as means +\- SEM. No significant factors were detected in a 2-way ANOVA, using enhancer locations and genotype.

J. Density scatter plot of log10 number of intragenic enhancers versus log10 gene length for all genes in the genome. Spearman rho shown for the number of intragenic enhancers and gene length for all genes with at least 1 enhancer. ***, $p < 10^{-8}$.

K. Running-average plot of fold-change in intronic RNA expression in the MeCP2 KO or MeCP2 OE versus mCA/kb for genes containing enhancers (red line) and length-matched sets of genes that do not contain enhancers (gray lines). Mean fold-changes are plotted for bins of 201 genes sorted by mCA/kb with a 1-gene step (see methods).

L. Local correlation analysis correlating mCA/kb (left) and mCG/kb (right) for 1 kb windows in and around genes to intronic RNA fold-changes for the gene in the MeCP2 KO (top) and OE (bottom). Genes at least 75kb in length are analyzed to allow visualization of correlations in gene bodies. Genic windows of methylation go from the TSS to 75kb downstream.

M. Heatmap of correlation between fold-change in H3K27ac at intragenic regions and gene expression fold-change for MeCP2 KO and MeCP2 OE mice. Values are calculated as partial correlation for enhancers or control non-enhancer regions of the same size, removing the signal from the other class of element (see methods). Larger correlation for enhancers over control regions illustrates the link between enhancer regulation and transcriptional control.

Data from cerebral cortex of 7-10 week old animals. For MeCP2 KO: n=5 per genotype for H3K27ac, n=6 per genotype for RNA-seq; for MeCP2 OE: n=3 per genotype for H3K27ac, n= 5 per genotype for RNA-seq; n=2 wild-type for DNA methylation (Stroud et al., 2017). ATAC-seq peaks (Cusanovich et al., 2018). Note that some panels in C are repeated from Figure 4 to allow for comparisons.

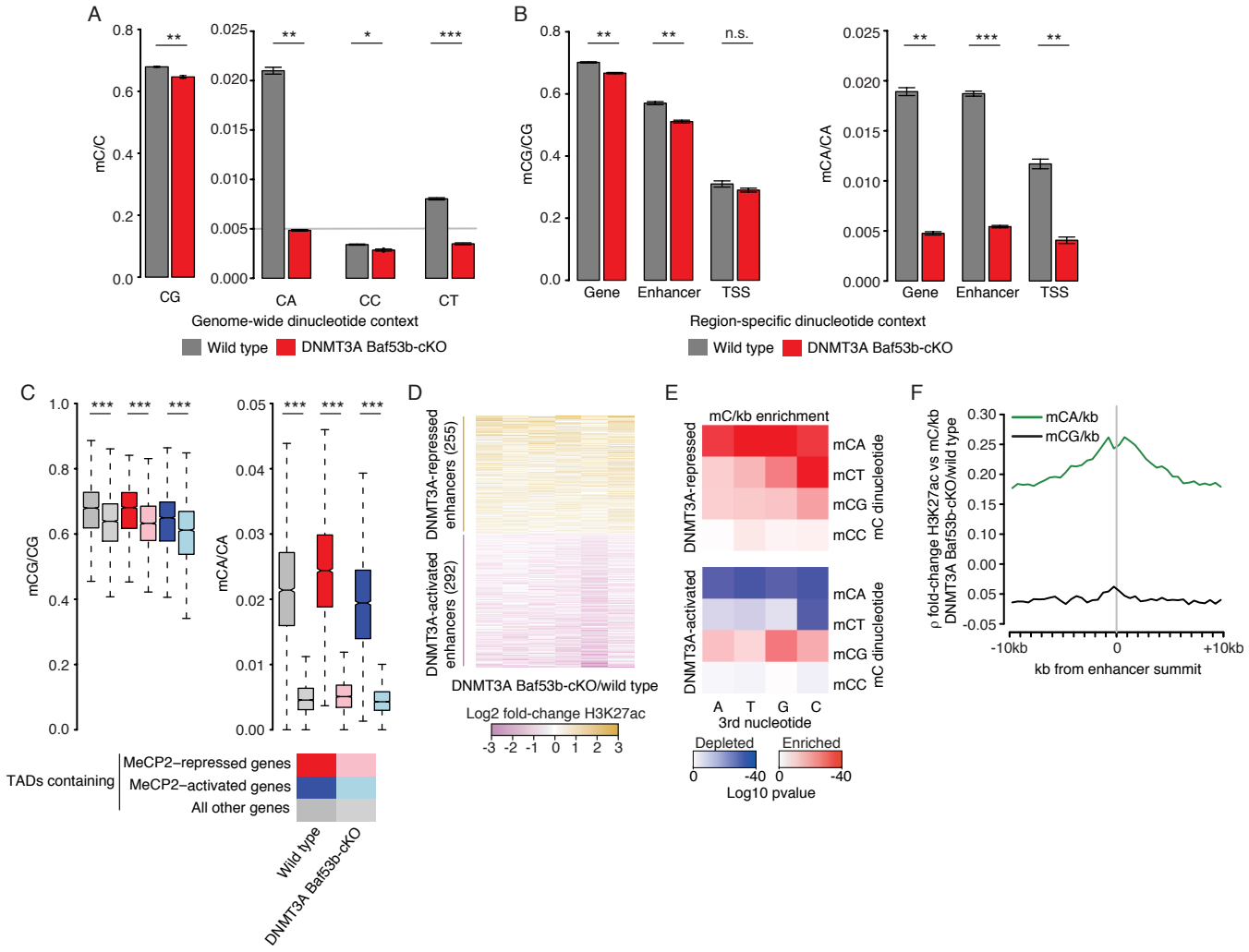

Figure S6. Transcriptomic and epigenomic analysis of DNMT3A Baf53b-cKO. Related to Figure 5.

A. Barplots of genome-wide methylation levels in the DNMT3A Baf53b-cKO at different CN dinucleotides. Data shown as means +\- SEM. *, $p < 0.05$, **, $p < 10^{-3}$; ***, $p < 10^{-8}$ two-tailed t-test.

B. Barplots of mCG (left) and mCA (right) levels in the DNMT3A Baf53b-cKO at genes, enhancers, and TSSs. Data shown as means +\- SEM. **, $p < 10^{-3}$; ***, $p < 10^{-8}$ two-tailed t-test.

C. Boxplots of mCG (left) and mCA (right) levels in the DNMT3A Baf53b-cKO within TADs that contain MeCP2-repressed genes, MeCP2-activated genes, or no dysregulated genes. ***, $p < 10^{-8}$ Wilcoxon rank-sum test.

D. Heatmap of H3K27ac fold-changes for enhancers detected as significantly dysregulated in DNMT3A Baf53b-cKO mice by edgeR analysis (see methods).

E. Heatmap of enrichment significance for the number of mC sites (mC/kb) within enhancers detected as significantly dysregulated in the DNMT3A Baf53b-cKO. Significance of enrichment or depletion was calculated by comparing occurrences of mC/kb for each trinucleotide in the 2kb region surrounding enhancers to resampled sets of enhancers that are not significantly changed but matched to changed enhancers for H3K27ac signal (see methods).

F. Plot of spearman correlations between H3K27ac fold-change at enhancers in the DNMT3A Baf53b-cKO and mC/kb levels in the wild-type brain for 500bp bins in and around the enhancers. Plots are centered at the summit of enhancer H3K27ac ChIP peaks.

Data from cerebral cortex of 7-10 week old animals. n=6 per genotype for Bisulfite-seq analysis, n=6 per genotype for H3K27ac.